Engineering Geology 202 (2016) xxx–xxx

Contents lists available at ScienceDirect

Engineering Geology

journal homepage: www.elsevier.com/locate/enggeo

Geoelectrical resistivity variations and lithological composition in coastal gypsum rocks: A case study from the Lesina Marina area (Apulia, southern Italy)

Vincenzo Festa [a], Simona Tripaldi [a,*], Agata Siniscalchi [a], Pasquale Acquafredda [a], Antonio Fiore [b], Daniela Mele [a], Gerardo Romano [a]

[a] Dipartimento di Scienze della Terra e Geoambientali, Università degli Studi di Bari Aldo Moro, Via E. Orabona, 4, 70125 Bari, Italy
[b] Autorità di Bacino della Puglia, c/o Innova Puglia S.P.A. (ex Tecnopolis Csata), Str. Prov. per Casamassima, Km 3, 70010 Valenzano, Bari, Italy

ARTICLE INFO

Article history:
Received 23 December 2014
Received in revised form 23 November 2015
Accepted 27 December 2015
Available online 30 December 2015

Keywords:
Evaporite karst
Gypsum
Petrography
Electrical resistivity tomography

ABSTRACT

The Lesina Marina village (Apulia, southern Italy) lies on an exotic rocky body basically composed of Triassic gypsum surrounded and covered by thin Quaternary sandy deposits. During the last two decades instability phenomena connected to gypsum dissolution and cover suffusion sinkholes occurred mainly along the Acquarotta canal and in the urbanized area.

In this study, electrical resistivity tomographies, field and petrographic observations have been carried out just ca. 300 m to the South of the residential area. The East–West striking geoelectrical profile has a length of 1900 m, intercepts two boreholes and crosscuts the Acquarotta canal. Close to the boreholes, higher resolution geoelectrical profiles, both perpendicular and parallel to the former, were performed. The two boreholes highlight the presence, from the top to the bottom, of Quaternary sandy deposits, coarse grained gypsum and layered finer grained gypsum. In correspondence, electrical resistivities are very low for the wet sandy deposits (up to 5 Ω·m), increase for coarse grained gypsum (20–120 Ω·m) and reach the maximum values for the layered finer grained gypsum (greater than 300 Ω·m).

The relationship between the electrical resistivity and the lithological composition of the studied rocks is strongly controlled by their fracturing and water saturation degree. Thus considering, the main geological features here recovered are the impermeable bedrock and the above rocky body involved by mineral transformations and karstification phenomena. Additionally, the anhydrite/gypsum transformation and the gypsum dissolution are related to the groundwater circulation and localized within massive coarse grained gypsum rocks. Therefore, the hazard related to karst processes involves both an area and a depth greater than those considered up to now.

1. Introduction

Ancient gypsum rocky bodies often show different portions characterized by a variety of both lithological composition (e.g. Testa and Lugli, 2000; Gündogan et al., 2005; Schreiber et al., 2007) and/or texture (e.g. Gündogan et al., 2008; Hildyard et al., 2009). This complexity (e.g. alternating gypsum, limestone and clayey layers, as well as the presence or the absence of intergranular matrix) is due to either the primary chemical and physical conditions of the evaporitic environments of deposition, or to the subsequent mineral transformations resulting from a complexity of factors during diagenesis (e.g. tectonics, burial, exhumation and weathering processes).

The ability of electrical resistivity tomography (ERT) method to assess subsurface property, in an evaporitic setting, should be enhanced by the excellent electrical contrast between the near surface air-filled or water/clay filled cavities and the host material. Nevertheless, overlapping resistivity ranges exist for a single sulfate rocky mass since the electrical resistivity depend on a wide range of the petrophysical parameters (structure, texture, temperature, mineralogy, water content, concentration and chemical composition of the fluids, etc). In order to investigate these parameters in ancient sulfate rocky bodies, ERT has been successfully applied even though in few cases of study (e.g. Guinea et al., 2010, 2012, 2014; Manoutsoglou et al., 2010, and references therein). Particularly interesting are the results reached by Guinea et al. (2012), which demonstrated a direct relationship between the electrical resistivity values and the contents of gypsum and anhydrite in sulfate rocks, quantifying the decreasing of resistivity with the increasing of the lutitic matrix embedding sulfate particles.

Lesina Marina is a village lying a few meters above sea level on the Fortore River coastal plain that extends along the northern Apulia Adriatic coastline (southern Italy; Fig. 1a and b). In this area, exotic Triassic gypsum rocks crop out on a very gentle ridge (e.g. Carella, 1963), surrounded and covered on its sides by relatively thin Quaternary

* Corresponding author.
E-mail address: simonatripaldi@geo.uniba.it (S. Tripaldi).

http://dx.doi.org/10.1016/j.enggeo.2015.12.026
0013-7952/

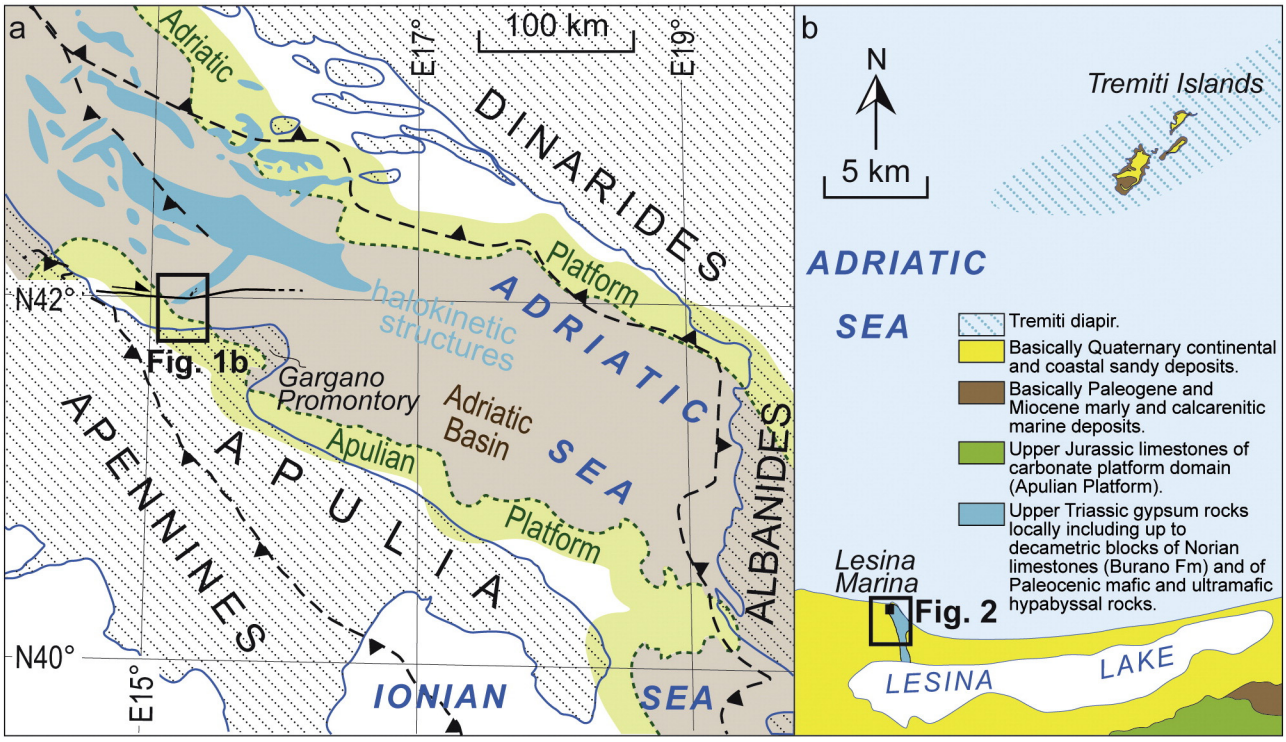

Fig. 1. (a) Schematic structural map of the Periadriatic region around the Adriatic Sea (after Zappaterra, 1990, 1994, modified). The Meso-Cenozoic paleogeographic position of the Adriatic Basin between the Apulian and Adriatic carbonate platforms is shown. The fronts of Apennines and Dinarides according to Scrocca (2006), and Fantoni and Franciosi (2010), respectively. The halokinetic structures are also indicated (after Geletti et al., 2008, modified). (b) Schematic geological map of northern Apulia, around the area of Lesina Marina village and of the Tremiti Islands (after Boni et al., 1969; Cremonini et al., 1971, modified); the location of the underlying halokinetic structure called Tremiti diapir is also indicated
After Festa et al. (2014), modified.

sandy deposits (Mastronuzzi and Sansò, 2012, and references therein; Figs. 1b and 2). Besides the uniqueness of these gypsum rocks in the surface geology of the southern Italy (e.g. Martinis and Pieri, 1964), their importance is also related to the large number of cover collapses and cover suffosion sinkholes that have been formed in the gypsum karst of the Lesina Marina area, thus impinging dangerously the residential area during the last two decades (e.g. Melidoro and Panaro, 2000; Fidelibus et al., 2011; Caggiano et al., 2012; Fig. 3a).

Melidoro and Panaro (2000) and Fidelibus et al. (2011) suggested that the changes in the hydrogeological functioning due to the Acquarotta canal (artificially excavated in 1930 in the gypsum rocky body, in order to connect the Lesina lagoon with the Adriatic Sea; Figs. 1b and 2) have favored both the erosion of the filling of cavities and the karstification processes, promoting the development of the sinkholes near the canal, especially along its western side. However, according to Campana and Fidelibus (2015), in the Lesina Marina area the evolution time of gypsum dissolution is much greater than human lifetime.

Previous studies were mainly focused within the urbanized area, and in the first 30 m in depth (Melidoro and Panaro, 2000; Selleri and Mastronuzzi, 2003; Fidelibus et al., 2011; Caggiano et al., 2012). Therefore, the extent of the karst system in depth and around the village is unknown.

The main objective of this study is to provide a wider and a deeper geological reconstruction. This reconstruction represents an essential tool to suggest a new framework of susceptibility to the possible occurrence of near-surface collapse phenomena, even outside the urbanized area. Indeed, sinkholes occurred not exclusively near and along the canal (e.g. Caggiano et al., 2012), and some clues for the happening of these phenomena, far from the canal, may be suggested by satellite images (Google Earth, 2013), consisting of sub-elliptical wetter soil compared to the surroundings (Fig. 3b). To this end, the electrical resistivity tomographies, field mapping and petrographic observations have been carried out. The results are discussed in relation to the outcomes of previous studies devoted to both the understanding of the collapse phenomena in the Lesina Marina area (e.g. Melidoro and Panaro, 2000; Fidelibus et al., 2011; Caggiano et al., 2012), and to ERT and petrophysical investigations on gypsum rocks (e.g. Guinea et al., 2010, 2012, 2014; Manoutsoglou et al., 2010).

2. Geological and hydrogeological setting

In the Adria Plate (sensu Channell et al., 1979), a narrow pelagic basin (the Adriatic Basin), flanked by carbonate platforms (the Apulian Platform, to the SW, and the Adriatic Platform, to the NE), developed during the Mesozoic, roughly occupying the same position of the present-day Adriatic Sea (Zappaterra, 1990, 1994; Bernoulli, 2001; Fig. 1a). The system made of these basinal and platform domains evolved as a consequence of early Jurassic rifting of an epeiric area dominated by the deposition of carbonates. It was rooted on Norian anhydrites and shallow-water limestones and dolostones, i.e., the Burano Fm, which overlie Permian continental deposits draping Hercynian basement (Ricchetti et al., 1988). Later, the basinal and platform domains were partially involved in the Tertiary shortening related to the Apennines and to the Dinarides–Albanides evolution. Near and along the front of these orogens, the evaporites belonging to the Burano Fm promoted diapirism, mostly during Neogene (e.g. Scrocca, 2006; Geletti et al., 2008; Festa et al., 2014, and references therein; Fig. 1a).

In the North of Apulia (Fig. 1a), in the Lesina Marina area, the cropping out of exotic Triassic gypsum rocks belonging to the Burano Fm (Fig. 1b), rose up from the deep anhydrite source (Cotecchia and Canitano, 1954; Bigazzi et al., 1996). According to Bigazzi et al. (1996), hydration of anhydrites, i.e., the formation of gypsum, possibly occurred after their uprise. Up to decametric blocks of Paleocenic mafic and ultramafic hypabyssal rocks (De Fino et al., 1983; Bigazzi et al., 1996), and Triassic limestones (e.g. Posenato et al., 1994), that locally crop out

Please cite this article as: Festa, V., et al., Geoelectrical resistivity variations and lithological composition in coastal gypsum rocks: A case study from the Lesina Marina..., Eng. Geol. (2016), http://dx.doi.org/10.1016/j.enggeo.2015.12.026

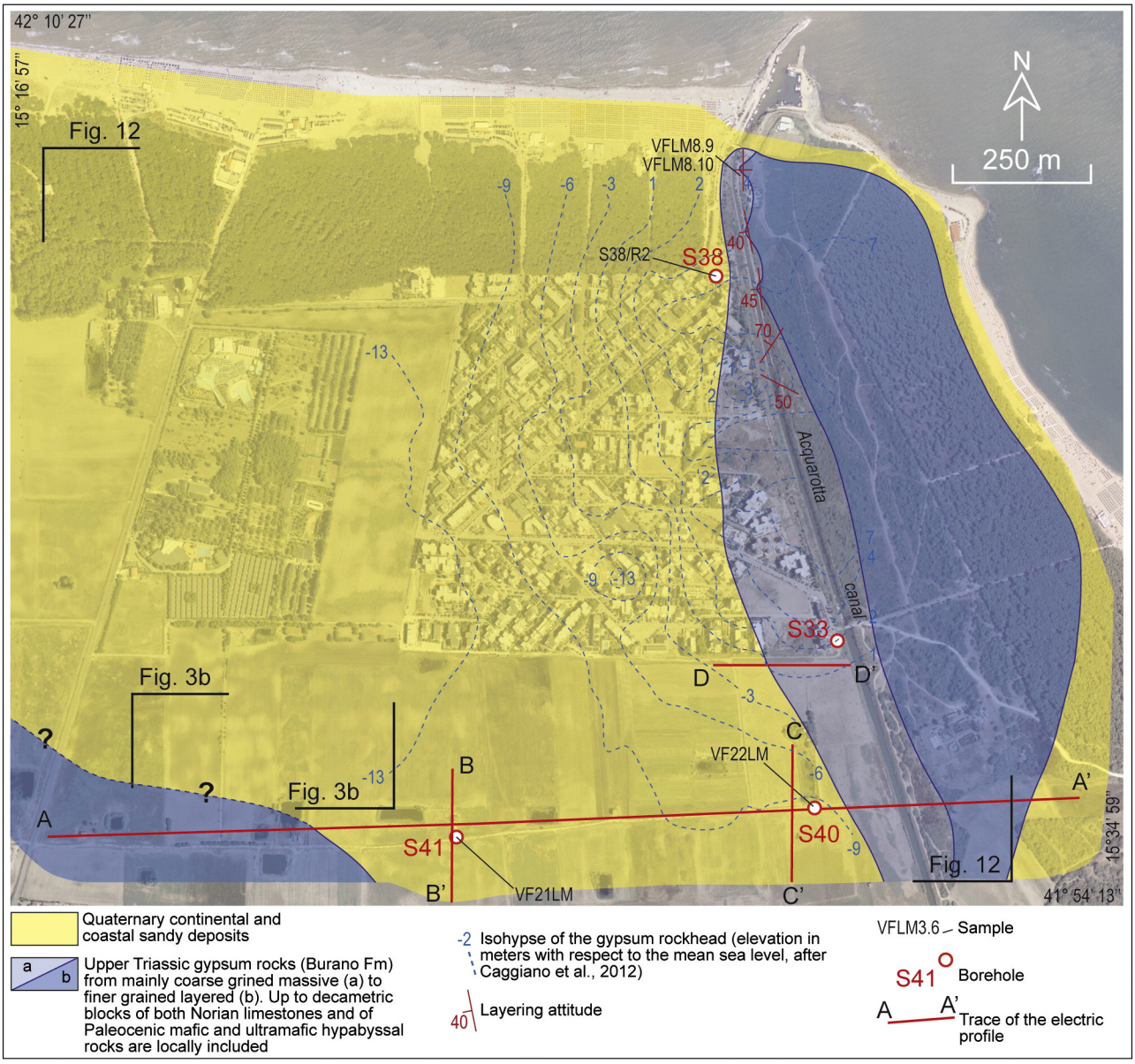

Fig. 2. Schematic geological map of the Lesina Marina village area.

Fig. 3. (a) Photograph of collapse sinkholes (the arrows indicate the marginal cracks) in the urbanized area of Lesina Marina (a sidewalk and a tennis court involved in the collapse can be identified). (b) Satellite images (Google Earth, 2013) on which sub-elliptical wetter soil (in dashed ellipses) can be appreciated in the south-western part of the Lesina Marina area (Fig. 2, for the location).

Please cite this article as: Festa, V., et al., Geoelectrical resistivity variations and lithological composition in coastal gypsum rocks: A case study from the Lesina Marina..., Eng. Geol. (2016), http://dx.doi.org/10.1016/j.enggeo.2015.12.026

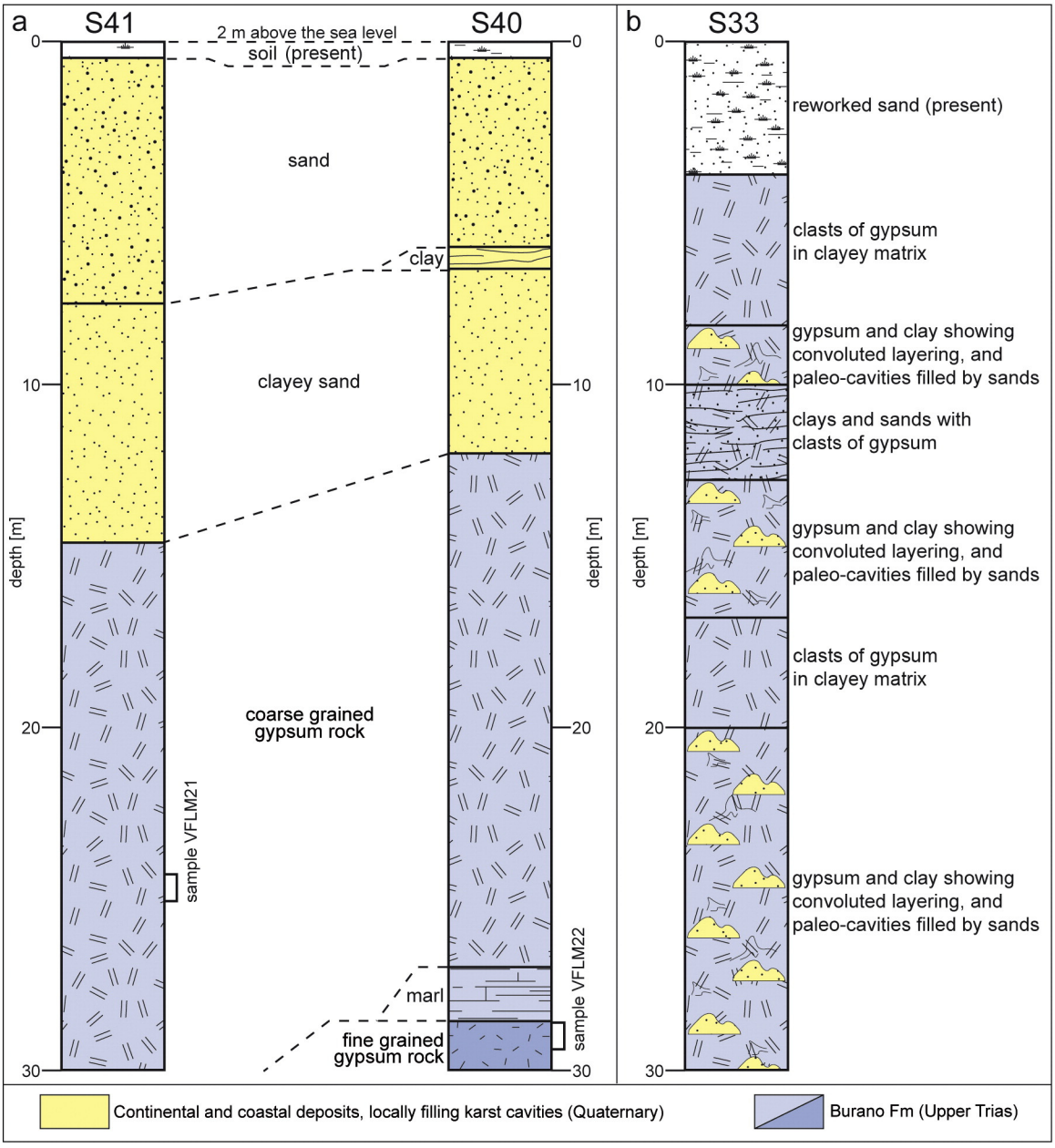

Fig. 4. (a) Reinterpreted stratigraphic logs of the S40 and S41 boreholes (Fig. 2, for the location). (b) Stratigraphic log of the S33 borehole (Fig. 2, for the location). Redrawn after Melidoro and Panaro (2000).

embedded in the gypsum rocks (e.g. Amendolagine et al., 1964), might have been dragged, from the depth, during ascent by diapirism of the gypsum body (Cotecchia and Canitano, 1954) or by tectonic squeezing of the anhydrites (Bigazzi et al., 1996).

The gypsum bedrock in the subsurface of Lesina Marina, where its top gently dips toward West up to ca. 13 m below sea level (Fig. 2; e.g. Caggiano et al., 2012), shows a high density of cavities, either dissolutional conduits or voids related to gravitational collapse processes. As observed in the first 30 m by borehole investigations, most of these cavities, up to metric in size, are partially or totally filled basically with sandy deposits derived from the overlying Quaternary sedimentary cover (Melidoro and Panaro, 2000). Melidoro and Panaro (2000) and Fidelibus et al. (2011) suggested that most of the cavities originated during paleo-karst processes; these processes were activated due to the Last Glacial Maximum, when the sea level in the Adriatic coast was around 130 m below its current position. Therefore the presence of the cavities has been hypothesized well below the investigated first 30 m in depth (Fidelibus et al., 2011). In addition, according to Melidoro and Panaro (2000), some cavities may be related to a probable karst undercover genesis and evolution. In this regard, karst processes in progress have not been excluded also by Selleri and Mastronuzzi (2003) and by Fidelibus et al. (2011), due to the excess of calcium and sulfate concentrations in the groundwater. In the Lesina Marina area, the aquifer occupies the karst gypsum bedrock and, partially, the Quaternary sandy deposits; piezometric records in the urbanized area show that the water table is located 1.5 m above sea level (i.e. ca. 6.5 m below the topographic surface) in the western sector, to 0.5 m above sea level (i.e. ca. 9.5 m below the topographic surface) near the Acquarotta canal. The geometry of the piezometric surface of the karst aquifer, gently dipping toward the East, indicates a dominant W–E groundwater flow direction toward the draining Acquarotta canal (Melidoro and Panaro, 2000; Fidelibus et al., 2011; Caggiano et al., 2012). In addition, the water table pulsates according to the tidal oscillations that are in the order of ca. 0.40 m (Melidoro and Panaro, 2000;

Fidelibus et al., 2011). The active dissolution of the gypsum bedrock must be the origin of the previously mentioned calcium and sulfate concentrations, from three to four times and two times higher, respectively, than expected from simple fresh water and seawater mixing (Fidelibus et al., 2011).

3. Material and methods

3.1. Field, petrographic and borehole investigations

For a convincing ERT interpretation, the field mapping, the petrographic observations on sulfate rock samples, and the reinterpretation of logs from available cores of borehole (Fig. 4a) have been carried out; in addition, some remarks on the secondary porosity of the gypsum rocky body have been derived.

Since the Quaternary sandy deposits are very poorly exposed, although their presence is well constrained by many holes drilled in the area (Melidoro and Panaro, 2000; Fidelibus et al., 2011), the geological mapping focused on the N–S striking gentle ridge made by Upper Triassic gypsum rocks, well exposed especially along the northern part of the Acquarotta canal (Fig. 2). The field mapping and the sampling for the petrographic investigations on the sulfate rocks benefited from the available cores from boreholes S41, S40 and S38 (Fig. 2, for their location), drilled up to 30 m in depth on behalf of the "Basin Authority of Apulia" institution.

For the petrographic investigations on sulfate rocks, the samples VFLM8.9 and VFLM8.10 were collected along the Acquarotta canal (Fig. 2, for their location), whereas samples VFLM21, VFLM22, and S38/32 were collected at 25 m, 29.5 m and 25 m in depth from cores of boreholes S41, S40 and S38, respectively (Figs. 2 and 4a, for their location).

Optical microscope (polarized transmitted light) observations on thin sections prepared from these samples have been performed in order to distinguish gypsum from anhydrite, and the intergranular lutite; to measure the percentage of intergranular lutite the image analysis toolbox JMicrovision 1.2.7 (Nicolas, 2009) was used. The lutite was evidenced from the gypsum crystals by binary threshold selection and then its area was determined.

Finally, in order to detect the secondary porosity related to fracturing in the gypsum bedrock, the Rock Quality Designation (RQD; Deere, 1963) was determined both on the available cores of boreholes and along the eastern slope of the Acquarotta canal, through the scan-line method (e.g. Brady and Brown, 2006).

3.2. Resistivity data acquisition and processing

For the present study four ERT profiles (AA′, BB′, CC′, DD′; Fig. 2 for the location) were carried out using the multi-electrode Syscal R2 system with 48 electrodes. Detailed reviews on basic principles of the resistivity method and its numerous practical applications can be found in Loke et al. (2013), Slater (2007) and Revil et al. (2012).

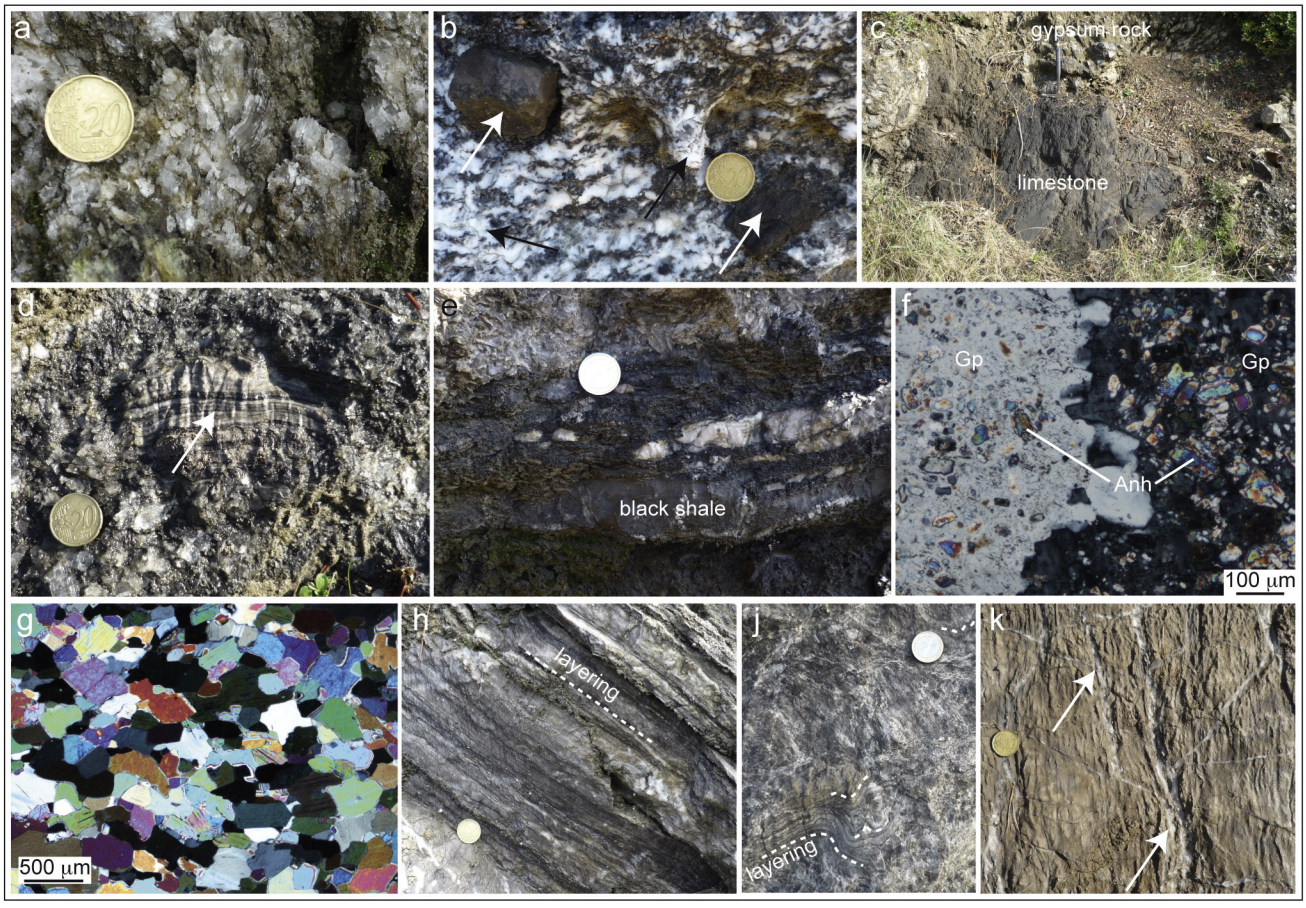

Fig. 5. (a) Colorless large crystals of gypsum. The cleavage planes can be also appreciated. (b) Centimetric clasts of Paleocenic ultramafic rocks (white arrows) within the massive gypsum matrix, in which white gypsum crystals (black arrows) can be recognized. (c) Metric block of Triassic limestone within the massive gypsum rocks. (d) Centimetric fragment of finer grained layered gypsum rock (white arrow) within the massive gypsum matrix. (e) Centimeter-thick layer of black shale within the massive gypsum rocks. (f) Thin section micrograph (crossed polars) of the sample VFLM8.9 (see Fig. 3 for its location) showing gypsum (Gp) poikilocrystals with small inclusions of anhydrite (Anh); mineral abbreviations after Kretz (1983). (g) Thin section micrograph (crossed polars) of the sample S38/32 showing only anhydrite crystals. (h) Whitish to dark grayish millimeter- to centimeter-thick layers with plane parallel geometry in finer grained gypsum rocks. (j) Convolute layers in finer grained gypsum rocks. (k) Fractures filled by secondary gypsum (white arrows), crosscutting gypsum rocks.

Please cite this article as: Festa, V., et al., Geoelectrical resistivity variations and lithological composition in coastal gypsum rocks: A case study from the Lesina Marina..., Eng. Geol. (2016), http://dx.doi.org/10.1016/j.enggeo.2015.12.026

The acquisitions were always performed with two traditional arrays, the dipole–dipole (DD) and Wenner–Schlumberger (WS). The former should provide a better lateral resolution while the latter should provide a better vertical resolution. For a comprehensive review of the arrays' characteristics in terms of resolution, depth of investigation and noise see Dahlin and Zhou (2004).

The profile AA′ strikes E–W intercepts the boreholes S40 and S41 and crosscuts perpendicularly the Acquarotta canal (Fig. 2). Stainless steel electrodes were plugged into the ground at a fixed spacing of 20 m using 48 electrodes along three successive segments with the superposition of 24 electrodes. These three successive layouts returned a final profile with a total length of 1900 m. A dipole length up to 3 'a' and a dipole separation factor 'n' up to 8 and 7 were used for WS and DD respectively (1650 WS and 2325 DD measurements). It is worth to note that during the acquisition process off-line structures, such as small ponds or sub-elliptical (in plan view) wetter soil (e.g. Fig. 3b) have been found to the W and in the central part of AA′ profile, while several sinkholes have been found to the E. Nevertheless, the 2-D approximation is easily acceptable since the profile is perpendicular to the elongation of the main geological bodies.

Profiles BB′ and CC′ strike N–S and were performed close to boreholes S41 and S40 respectively, and perpendicularly to AA′ (Fig. 2). Profile DD′ strikes W–E and was performed just outside the urbanized area, near the Acquarotta canal, and in proximity of borehole S33 (Fig. 2, for the location) whose data are available in Melidoro and Panaro (2000; Fig. 4b). These three profiles were carried out using 48 electrodes with a fixed spacing of 5 m and measure 235 m in length. A dipole length up to 3 'a' and a dipole separation factor 'n' up to 6 (486 and 600 measurements for WS and DD respectively) were used. The twofold purpose of BB′, CC′ and DD′ is: a) gaining high resolution resistivity data in the first 30 m so as to strictly study the correlation between resistivity and borehole data; b) evaluating the trend of gypsum rockhead depth in spatial continuity with the already existing data in the urbanized area. Close to DD′ profile, where electrical conductivity (and concentration of ions) of permeating water are available from borehole S33, insight into the distribution of resistivity values is given using the Hashin and Shtrikman (1963) model. This physical parametrization allows to define the maximum and minimum values that can be observed for electrical properties of a multicomponent medium (phases composed by distinct minerals and/or fluids). All the components of the system are assumed to be isotropic and homogeneous. In the present work, the proximity to the Acquarotta canal indicates that the main conductive phase is brine water, and deviation from rigorous HS (Hashin and Shtrikman) bounds might occur if the assumption of isotropy and homogeneity fail (depending on, e.g., density, shape and orientation of fractures/cracks and their water content). Numerical approaches, which take into account different geometries of fractures bearing conductive fluids, show that major departures from HS resistivity lower bound occur in the presence of low porosity and high anisotropic fractures; otherwise results converge to the HS model (eg., Berryman and Hoversten, 2013; Bigalke, 2000). In our context, the aim is to study the dual contribution of two conductive phases (water and lutite), rather than rigorously measure individual quantities. With all due cautions, the use of the HS model seems adequate to this end. Before running inversions, bad data were excluded from all the datasets. After obvious outlier removal, we observed the resistivity data as a profile plot and their percentage errors computed on the different cycles of current injection used in the stacking procedure. Data characterized both by abrupt resistivity variations and large errors were rejected. In so doing, after rejection, the maximum percentage error was: for BB′ datasets 2.6% (WS) and 5.7% (DD); for CC′ dataset 1.8% (WS) and 6.8% (DD); for DD′ dataset 1.1% (WS) and 4.5% (DD). For profile AA′ the error cutoff value was chosen considering also the analysis performed on repeated measurements belonging to overlapping segments. The percentage errors related to repeated apparent resistivity measurements are almost Gaussian distributed with zero mean and a standard deviation of 10% (WS) and 15% (DD). Such values were chosen as error cut off, thus, data affected by higher percentage errors during the stacking procedure were rejected also by considering that an error overestimation could lead to a gross smoothing of the model. For the repeated points, however, we kept data with smaller errors; data with dipole separation factor 'n' higher than 6 were removed from the DD dataset. Finally, for each profile, a dataset WS + DD which combines WS and DD experimental measurements was arranged. The resistivity data of each dataset (WS, DD, WS + DD) were inverted with RES2DINV (Geotomo Software, Loke and Barker, 1996). Despite the very poorly pronounced morphologic variations (maximum gradient of 4 m above sea level along the AA′ profile), topography was included in the inversion process.

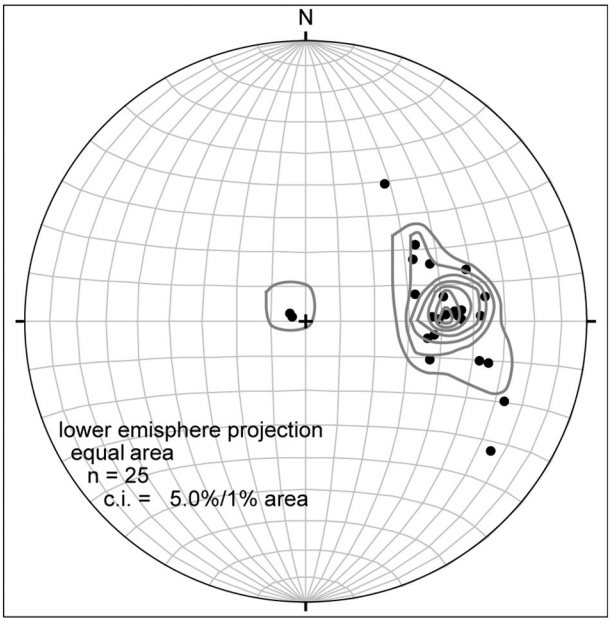

Fig. 6. Stereographic projection of poles to layering within gypsum rocks. The data were processed with Stereonet OSX Stereonet (Cardozo and Allmendinger, 2013).

The WS models have the lowest rms values and give a deeper image of the subsoil, but tend to be smooth masking targets of interest.

The DD models have the highest RMS values but provide much more detailed subsurface information. Indeed, among standard arrays, DD is the most advocated for the study of lateral resistivity contrast, cavities and cover–collapse sinkhole (Griffiths and Barker, 1993; Zhou et al., 2000; Nyquist et al., 2007).

The mixed WS + DD models provide an investigation depth analogous to the WS one and they are similar to the better detailed DD models. Although mixed array is less used, due to the significant increase in data collection effort, experiences reported in literature witness its higher effectiveness in similar conditions (Zhou et al., 2002; Manoutsoglou et al., 2010), likely because of the high density data coverage.

Considering all this, among the resulting models, we chose the WS + DD models with the smoothness-constrained least-squares method (de Groot-Hedlin and Constable, 1990; Loke et al., 2003) as the best compromise between DD and WS ones.

The presented resistivity models are characterized by a RMS of 12.6, 6.1 and 5.3 and 6.5 for models AA′, BB′, CC′ and DD′ respectively. Although the RMS error of the AA′ inverted resistivity profile is rather high, this could be blamed on the amount of data points and to the large resistivity variations in the data. In order to evaluate the zone of the inverted model that can be interpreted with confidence, the resolution per unit area contour line (0.05), computed by the RES2DINV software, will be overlaid on the resistivity model. In the resolution

Please cite this article as: Festa, V., et al., Geoelectrical resistivity variations and lithological composition in coastal gypsum rocks: A case study from the Lesina Marina..., Eng. Geol. (2016), http://dx.doi.org/10.1016/j.enggeo.2015.12.026

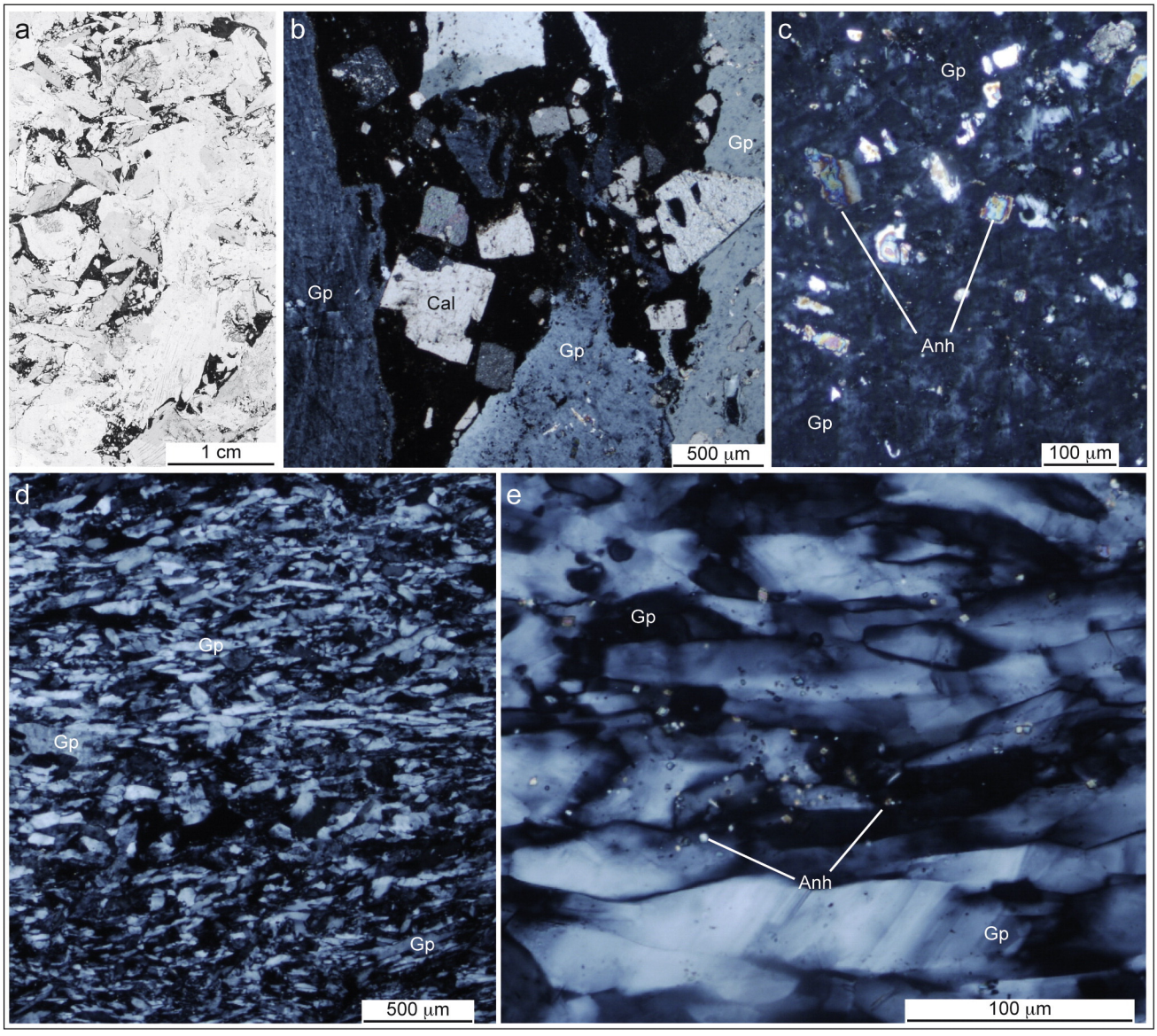

Fig. 7. (a) Thin section micrograph (plane polarized light) of the sample VFLM21 showing intergranular blackish lutite between whitish gypsum crystals. (b) Thin section micrograph (crossed polars) of the sample VFLM21 exhibiting euhedral and subhedral calcite (Cal) crystals within the blackish lutite and between large gypsum (Gp) crystals. (c) Thin section micrograph (crossed polars) of the sample VFLM21 illustrating a poikiloblast of gypsum (Gp) with inclusions of anhydrite (Anh). (d) Thin section micrograph (crossed polars) of the sample VFLM22 in which elongated gypsum (Gp) crystals preferentially oriented can be observed. (e) Thin section micrograph (crossed polars) of the sample VFLM22 in which very small anhydrite (Anh) crystals can be appreciated in fine grained gypsum (Gp). Mineral abbreviations after Kretz (1983).

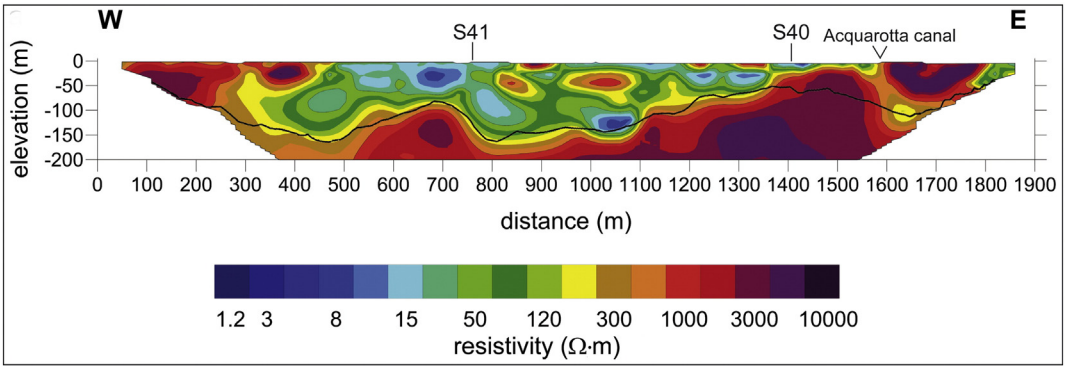

Fig. 8. Recovered AA′ resistivity model across the boreholes S40 and S41 (Fig. 2, for the location). The black line indicates the resolution per unit area contour line of 0.05.

Please cite this article as: Festa, V., et al., Geoelectrical resistivity variations and lithological composition in coastal gypsum rocks: A case study from the Lesina Marina..., Eng. Geol. (2016), http://dx.doi.org/10.1016/j.enggeo.2015.12.026

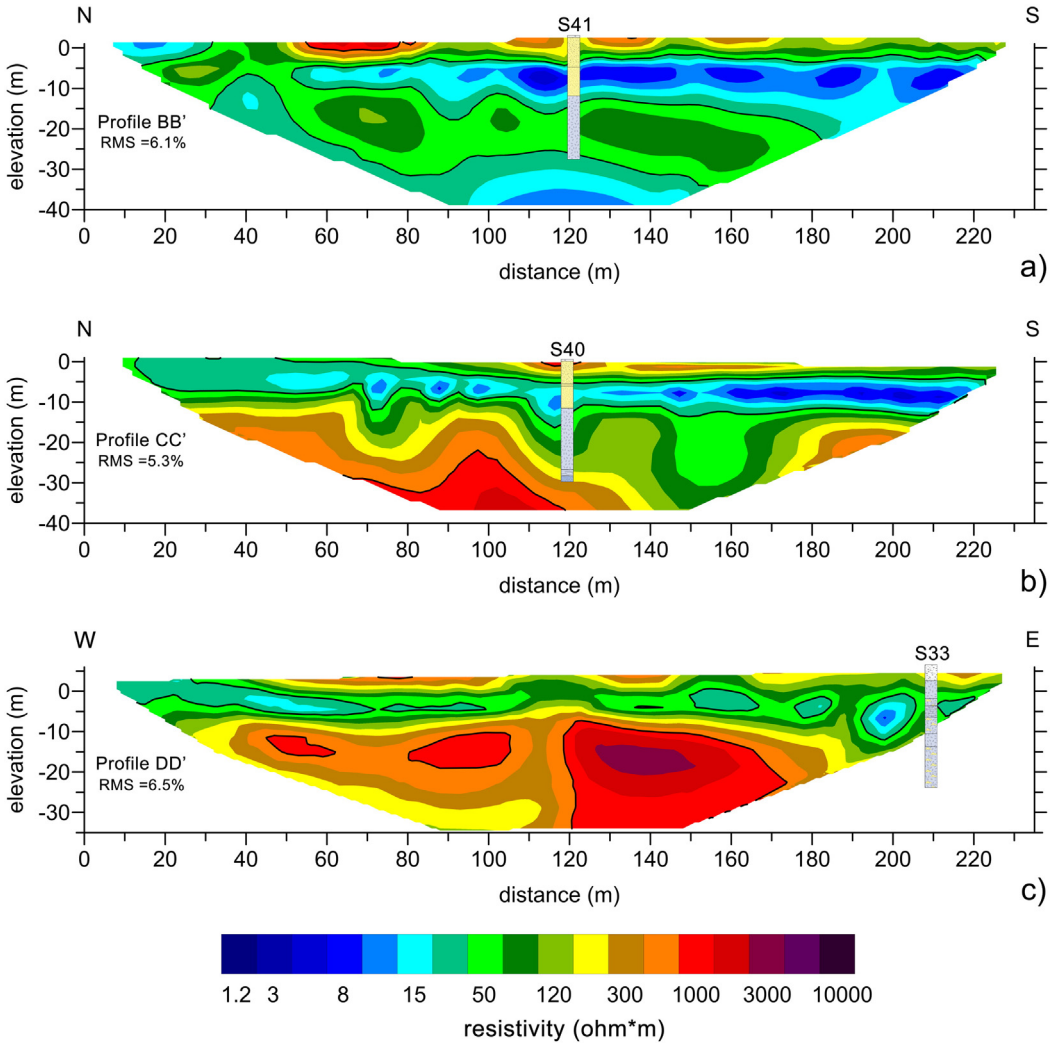

Fig. 9. Recovered resistivity models of profiles BB′, CC′, and DD′ (Fig. 2, for the location).

per unit area the model resolution is normalized by the cross-sectional area of the model block, thus depends on the model discretization. The resolution per unit area contour line may be regarded as a cut-off value below which electrical structures should be interpreted with caution, similarly as Robert et al. (2011) did with the sensitivity appraisal tool. For a quantitative comparison of different image appraisal indicators see Caterina et al. (2013).

4. Results

4.1. Field and petrographic observations

Along the northern part of the Acquarotta canal two sectors with elongated shape, ca. North–South striking in the map view, have been identified on the basis of the dominant lithotype: the western, dominated by massive coarse grained gypsum rocks, and the eastern, dominated by layered finer grained gypsum rocks (Fig. 2).

Within the massive portion, an intergranular lutite is often present between the larger gypsum crystals, which are euhedral or subhedral. The individual crystals, typically colorless or selenitic and with a good cleavage, reach a maximum size of 2–3 cm (Fig. 5a); white gypsum is locally present as well (Fig. 5b). Centimetric to metric in size fragments of both Paleocenic mafic to ultramafic hypabyssal rocks and Triassic limestones, as well as of finer grained layered gypsum rocks, locally crop out embedded in the massive gypsum matrix (Fig. 5b, c and d, respectively).

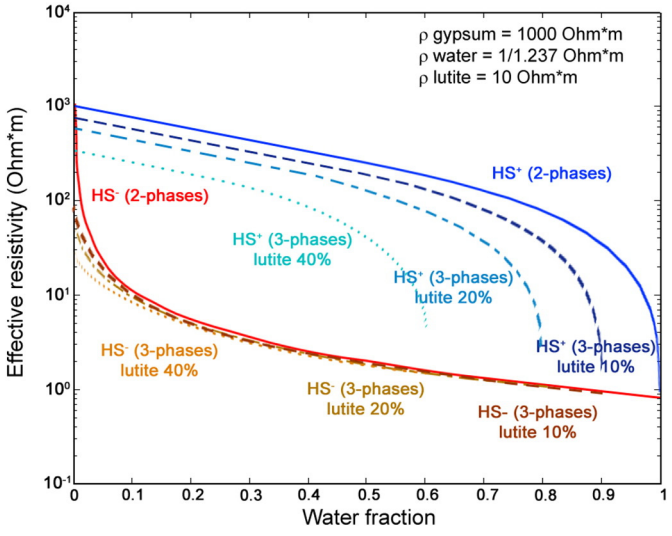

Fig. 10. Hashin–Shtrikman models calculated for the case of gypsum–water (2-phases modeling) and gypsum–water–lutite (3-phase modeling) obtained varying the lutite contents.

Please cite this article as: Festa, V., et al., Geoelectrical resistivity variations and lithological composition in coastal gypsum rocks: A case study from the Lesina Marina..., Eng. Geol. (2016), http://dx.doi.org/10.1016/j.enggeo.2015.12.026

Sometimes, a layering in the gypsum massive portion is highlighted by some centimeter-thick layers of black shales (Fig. 5e). Optical microscope (polarized transmitted light) observations of thin sections (on samples VFLM8.9 and VFLM8.10 collected along the Acquarotta canal; see Fig. 2 for their location) reveal that gypsum crystals, usually characterized by low birefringence with first order gray interference colors, are represented by poikilocrystals with small inclusions of anhydrite (Fig. 5f). Otherwise, bright, second order interference colors typically distinguish the anhydrite crystals (Fig. 5f, and g). In addition, it is worth to note that in the subsurface of Lesina Marina village, rocks completely formed by anhydrite (Fig. 5g) were found in the sampled core of borehole S38 (sample S38/32; Fig. 2 for the location). The relationships between gypsum crystals and anhydrite inclusions (e.g. Fig. 5f) indicate that gypsum is secondary and that formed by hydration processes at the expense of the original anhydrite, locally still preserved and not yet involved in the anhydrite vs. gypsum transformation (e.g. Fig. 5g).

In finer grained gypsum rocks the layering is well developed and characterized by an alternation of whitish to dark grayish millimeter- to centimeter-thick layers that exhibit a plane parallel geometry (Fig. 5h); sometimes a chaotic convolute geometry is shown by this layers (Fig. 5j). The layered gypsum rocks, as well as the massive gypsum ones, are crosscutted by a network of centimeter-thick fractures filled by secondary gypsum (Fig. 5k). As shown in Fig. 6, the layering of gypsum rocks dips westward on average, with a mean plunge of 48°.

Boreholes S40 and S41 indicate that the contact between the above Quaternary sandy deposits and the underlying gypsum rocks is located at 10 m and 12 m below sea level, respectively (Fig. 4). In addition, while the massive coarse grained gypsum rocks dominate until the bottom of the borehole S41 (30 m in depth), a thickness of ca. 15 m of these rocks have been drilled in the borehole S40, before reaching the layered finer grained gypsum rocks, which dominate until the bottom (30 m in depth; Fig. 4a).

RQD of 60%, determined both on the available cores of boreholes and along the eastern slope of the Acquarotta canal, indicates a "fair" quality (Deere, 1963), due to fracturation, for the massive coarse grained gypsum rock body.

Similarly to what was observed on the cropping out massive coarse grained gypsum rocks, the thin sections of sample VFLM21 clearly show intergranular lutite between the larger gypsum crystals (Fig. 7a and b). In addition, gypsum crystals are often represented by poikilocrystals with inclusions of anhydrite (Fig. 7c). As shown in the micrograph of Fig. 7b, within the lutite, euhedral to subhedral calcite crystals are typically present. The percentage of lutite, measured on three thin sections from sample VFLM21, corresponds to 20%.

The thin sections of sample VFLM22, which concerns the layered finer grained gypsum rocks, exhibit elongated gypsum crystals preferentially oriented as the layering (Fig. 7d). In addition, it is worth to note that very small anhydrite crystals can be also found as inclusions in the fine gypsum grains (Fig. 7e). Accordingly, although with less common evidences with respect to the clear relationships between gypsum crystals and anhydrite inclusions in the massive rocks (e.g. Figs. 5f and 7c), even for the layered finer grained gypsum rocks the growth of gypsum, as product of the hydration of the original anhydrite, cannot be excluded.

4.2. Resistivity models

Within model AA′, the resistivity values vary within a range of four orders of magnitude (Fig. 8). On the whole, the model images a subsoil consisting of a central sector (from ca. 250 m up to the Acquarotta canal, eastward) characterized by medium-low resistivity values (about 50 Ω·m) and confined to the base and laterally by more resistive material. Within this sector there are very resistive local anomalies (1000–3000 Ω·m) as well as very conductive ones (1–10 Ω·m). The transition to the resistive materials is marked by strong, West-dipping resistivity gradients, and shows a wavy shape in depth. In addition, an area with high resistivity values (>300 Ω·m) has been detected to the West. Here, two shallow resistive anomalies (>3000 Ω·m) are present at about 50 and 25 m of depth at distances of 150 m and 400 m, eastward, respectively. In the subsurface of the Acquarotta canal, a conductive subvertical anomaly interposes within the recovered higher resistive materials.

The black line in Fig. 8 represents the resolution per unit area contour line 0.05. As it can be noticed, the resolution is not laterally constant because it worsens both in correspondence to the higher resistive basement and the decrease of data density points, due to the acquisition layout. This behavior is plausible since current flow lines tend to be concentrated in conductive volumes (e.g. Hermans et al., 2012).

The BB′ resistivity model (Fig. 9a) shows a narrower resistivity range, with very conductive electrical layers (below 15 Ω·m) alternated along with intermediate resistive ones (averaging around 120 Ω·m). These layers slightly deepen toward the South. Borehole S41 reports the presence of sandy material up to a depth of 14.5 m. In particular, from 7.8 to 14.5 m, saturated clayey sand is characterized by the lowest resistivity values (below 15 Ω·m). The transition from clayey sand to gypsum (thickness of 0.5 m) is characterized by gypsum fragments embedded in clayey sands which is also water saturated. It follows coarse grain gypsum up to a depth of 30 m, characterized by resistivity values ranging from 20 to 120 Ω·m.

The CC′ resistivity model (Fig. 9b) shows wider resistivity variations than BB′, with a sandwiched conductive layer (5 to 15 Ω·m) located at a few meters of depth. The bottom of this layer has an irregular shape, like an erosional horizon, and local anomalies are present at a distance of 70, 115, and 155 m. Below, a resistive layer is present. As for profile BB′, electrical layers slightly deepen toward the South. Borehole S40 reports the presence of sandy material up to a depth of 12 m cut off from a lens of clay at about 6 m. From 6.6 to 12 m, saturated clayey sands are characterized by the lowest resistivity values (below 15 Ω·m). The gypsum rockhead is found at 12 m and presents a high degree of alteration at a thickness of 0.8 m. Further down, coarse grain gypsum is characterized by resistivity values ranging from 50 to 120 Ω·m up to 27 m. In the bottom, where marl and finer grained gypsum are found, a marked resistivity increase (up to 400 Ω·m) can be observed.

The DD′ resistivity model (Fig. 9c) generally shows a higher resistivity trend. In the shallowest part of the model, a conductive layer lies

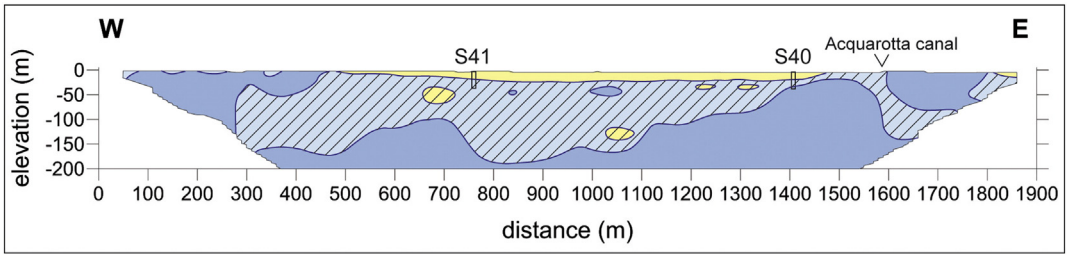

Fig. 11. Geological interpretation of the resistivity model AA′ (Fig. 8). Legend as in Fig. 2. Filling with inclined lines indicates the rocky body dominated by wet massive coarse grained gypsum, with both cavities filled by water saturated sandy deposits, and impermeable portions dominated by anhydrite.

Please cite this article as: Festa, V., et al., Geoelectrical resistivity variations and lithological composition in coastal gypsum rocks: A case study from the Lesina Marina..., Eng. Geol. (2016), http://dx.doi.org/10.1016/j.enggeo.2015.12.026

over a more resistive one; within the shallow conductive layer, resistivity values range from 10 to 100 Ω·m. In borehole S33, the thickness of reworked sands is about 4 m, the piezometric surface is located at 0.8 m and the gypsum rockhead is found at 2 m above sea level (Melidoro and Panaro, 2000; Fidelibus et al., 2011). Along our profile, gypsum rockhead is found at 1 m above sea level (Caggiano et al., 2012). Thus, the piezometric surface is hosted inside the top of gypsum rocks, locally lowering the resistivity of at least one order of magnitude with respect to the underlying resistive bedrock. Bedrock high resistivity values, above 1000 Ω·m, are mainly confined on the Eastern side of the model. Water sample at 3.5 m b.s.l. in borehole S33 has a conductivity of 1.237 S/m (Fidelibus et al., 2011); in the same range of depth, a resistivity drop (10 Ω·m) is reached in the eastern side of the model.

Two- and three-phase HS modeling was performed in order to estimate the relative contributions of the water–gypsum and water–lutite–gypsum systems. Since the HS mixing model considers a relatively homogeneous distribution of the phases, in this case we consider that it might be a valuable tool by considering a diffuse and interconnected fracturing/crack system rather than single isolated fractures. Moreover, the water conductivity values lower notably only on the west side of the urbanized area (far from the Acquarotta canal and from DD′ profile). Results show that in the three-phase system, the water and lutite contents have a different grade of influence on the effective resistivity with respect to the upper and lower bounds (Fig. 10). These bounds represent the theoretical maximum (upper bound) and minimum (lower bound) electrical resistivity values that any material, formed of n-different phases with a certain fraction, can display. In the lower bound, the resistivity is dominated by the water content since a 10% fraction determines resistivity values (about 10 Ω·m) comparable to the observed ones in the model. In the upper bound, the resistivity is more sensible to the lutite content, but to achieve resistivities of 10 Ω·m, a very low gypsum fraction is required which doesn't seem compatible with our borehole data.

Summarizing, all the resistivity models image a subsurface settled below the piezometric surface and hosting water saturated rocks. Where the piezometric surface intercepts the Quaternary sedimentary cover, the lowest resistivity values (up to 5 Ω·m) are found in correspondence to saturated clayey sands (Fig. 9a and b). Where the piezometric surface intercepts the gypsum rockhead (Fig. 9c), the prevailing resistivity is about 50 Ω·m and decreases, dropping up to 10 Ω·m, in the vicinity of the Acquarotta canal (Fig. 9c), where higher water salinity is present.

The contact between the Quaternary sandy cover and gypsum rockhead gently dips apparently toward South and the rockhead is composed of coarse grain gypsum (Fig. 9a and b).

Comparing models BB′, CC′ and DD′, the highest resistivity values, associable with gypsum rocks, are found both toward the North and the East.

In correspondence of boreholes S40 and S41, it is possible to assess that: a) saturated clayey sands are characterized by resistivity values ranging from 5 to 20 Ω·m; b) the coarse grain gypsum is characterized by resistivity values ranging from 20 to 120 Ω·m; and c) the finer grained gypsum is characterized by resistivity values ranging from 300 to 400 Ω·m.

It looks pretty clear that the abovementioned gypsum resistivity values are generally lower than those reported by literature (above 1000 Ω·m; e.g. Lugo et al., 2008; Manoutsoglou et al., 2010). Theoretical calculations, laboratory and field measurements conducted by Guinea

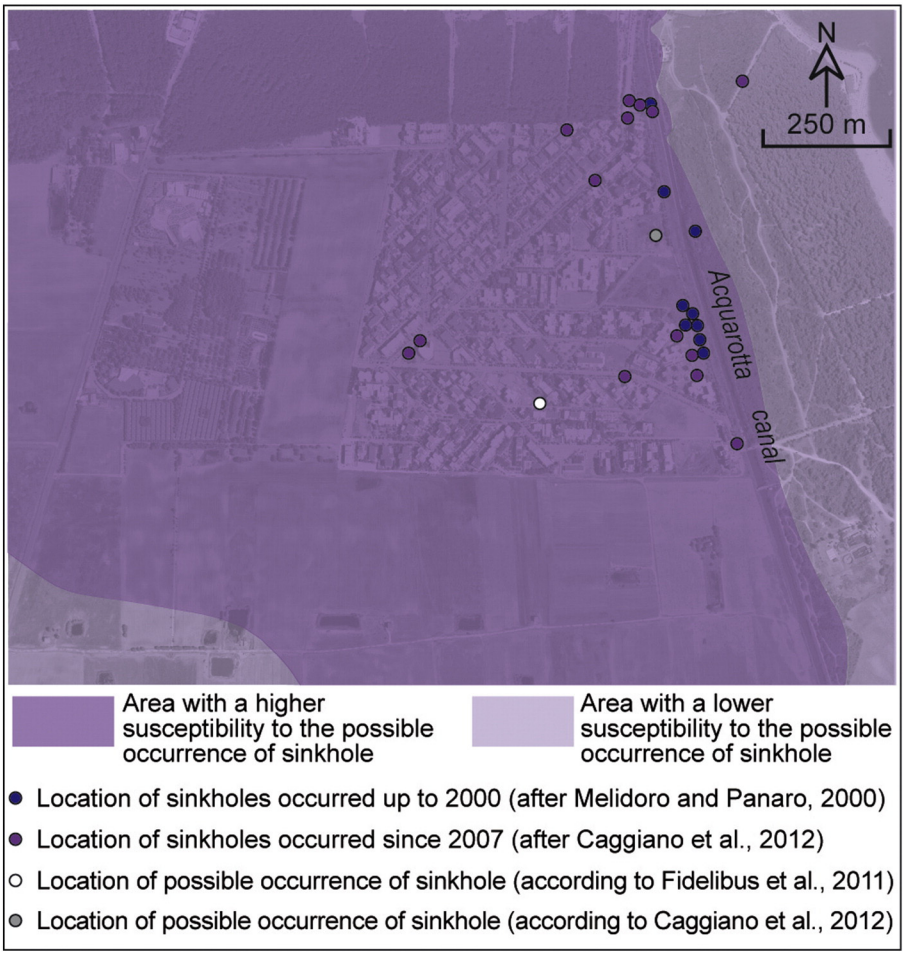

Fig. 12. Map of susceptibility to the possible occurrence of near-surface effects due to karst processes in the Lesina Marina area (Fig. 2, for its location, and text for further explanations).

Please cite this article as: Festa, V., et al., Geoelectrical resistivity variations and lithological composition in coastal gypsum rocks: A case study from the Lesina Marina..., Eng. Geol. (2016), http://dx.doi.org/10.1016/j.enggeo.2015.12.026

et al. (2010, 2012) correlate resistivity decreasing to variation in lithological composition. When gypsum and anhydrite have a purity close to 100%, resistivity ranges from 700 to 1000 Ω·m and from 2500 to 10^4 Ω·m, respectively; when the matrix (i.e., lutite) content in the gypsum rock is higher than 45% resistivity ranges from 100 to 10 Ω·m as the percentage of lutite increases from 45 to 100%, regardless of the differences in the composition (different combinations of gypsum and anhydrite) of the sulfate fraction (Guinea et al., 2010, 2012). The low content of lutite (20%; e.g. Fig. 7a) observed in our thin sections, does not justify the observed low resistivity values (below 20 Ω·m). Therefore, our results also seem strongly influenced by other parameters, such as fracturation, rather than lithological composition.

4.3. Large scale geological interpretation

The large scale resistivity investigation, performed along the profile AA′, witnesses a heterogeneous geological context. Despite the different scales of investigation, the gross resistivity variations in the AA′ model well match with the detailed ones reported in the intersection points with models BB′ and CC′; satisfactory similitude is also recovered in the resistivity distribution, in the first 40 m of depth, with the DD′ model located right to the West of Acquarotta canal (250 m north wise).

As can be observed in Figs. 8 and 11, the resistivity values over ca. 1000 Ω·m may be interpreted to be characteristic of gypsum rocks (dominated by finer grained ones) preserved from a significative degree of fracturation and water/clay infilling process. Higher resistivity values, could be related to a higher content of anhydrite. Indeed, the presence of portions represented by original anhydritic rocks should not be excluded within the layered finer grained gypsum rocks, as demonstrated by very small anhydrite inclusions in the fine gypsum grains (Fig. 7e). The eastern geological body composed of these rocks generally dips toward West (Figs. 8 and 11), as also confirmed by field data (Fig. 6). It shows a detected maximum thickness of ca. 170 m, and represents the bedrock of the Lesina Marina area (Fig. 11). Similar high resistivities, found in the south-western sector of the study area, could be reasonably associated with finer grained gypsum rocks and/or anhydrites (Fig. 2) since, in spite of the absence of outcrops, fragments of these rocks are widespread in the cultivated plowed field. Of course, other hypothesis cannot be excluded (e.g. the presence of a fault or of other lithological types). Nevertheless, whatever the origin of this western limit, it represents a boundary for the aggressive action of the gypsum dissolution processes.

To the East of the Acquarotta canal, where the AA′ intercepts both the cropping out of finer and of coarse grained gypsum (Fig. 2), very high resistivity values (500–3000 Ω·m) have been recovered. Here, the contact between coarse and finer grained gypsum is not resolved in terms of resistivity values (profile AA′, distance 1670 m). It is probably masked by the poor resolution in the first 30 m in depth that is not able to detect the exiguous thickness of the coarse grained gypsum. Indeed, here fields and borehole constraints indicate that the thickness of the coarse grain gypsum gently increases westwards from 0 m (in correspondence to the contact; Fig. 2) to 15 m (in correspondence to borehole S40; Fig. 4a). In addition, the superposition of very high resistivity features cannot be excluded in the coarse grained gypsum along the Acquarotta canal. The presence of both cavities, as reported by literature (Melidoro and Panaro, 2000; Selleri and Mastronuzzi, 2003; Fidelibus et al., 2011) and embedded fragments of mafic to ultramafic rocks, limestones, as well as of finer grained gypsum rocks (Fig. 5b, c and d, respectively) may be responsible for the bulk high resistivity values.

In the central sector of the geoelectrical profile (Fig. 8), above the high resistivity bedrock, the resistivities spanning a wide range of values, testify an heterogeneous and a complex geological framework. Here, the average resistivity values ranging from 50 to 120 Ω·m suggest the presence of a rocky body dominated by coarse grained gypsum, generally dipping toward West (Fig. 11). Its vertical thickness can somewhat be related to the position of the sea level in the Adriatic coast at the Last Glacial Maximum (e.g. Antonioli and Silenzi, 2007). Within this body, we interpret the occurrence of very conductive features as cavities filled basically with water saturated sandy/clayey sandy deposits, derived from the overlying Quaternary sedimentary cover. Accordingly, similar filled cavities have been abundantly found by borehole investigations in correspondence to the urbanized area (Melidoro and Panaro, 2000). As for the occurrence of very resistive features, we exclude the presence of empty cavities since below the water level, those cavities would be filled by water (relatively conductive) and would have lower resistivities. Thus, we suggest the presence of portions dominated by anhydrite. In this regard, anhydrite is most effectively transformed in gypsum (e.g. Figs. 5f and 7c) by groundwater circulating, probably starting from the Last Glacial Maximum, through interconnecting channels are localized along fractures and bedding planes. In this scenario, anhydrite rocks can still result and be locally preserved (e.g. Fig. 5g), giving high resistivities in isolated lens (Figs. 8 and 11). The gypsum dissolution or the anhydrite/gypsum transformation related to the groundwater circulation may have been spatially differentiated, also resulting in the wavy geometry of the boundary between coarse and finer grained gypsum rocks (Figs. 8 and 10). Furthermore, these phenomena have been favored in relation to the presence of the Acquarotta canal, thus affecting the permeability of the underlying finer grained gypsum rocky mass, where a conductive subvertical anomaly is embedded in the very resistive host (Figs. 8 and 11).

Summing up, the boundaries between overburdened water saturated sandy deposits, water-bearing fractured gypsum and impermeable fine grained gypsum/anhydrite bedrock, are electrically well distinguishable.

5. Discussion

Gypsum is generally characterized by low porosity and permeability, but due to the relatively high solubility of sulfate minerals, secondary porosity, such as fractures, can develop at different spatial scales (Guerrero et al., 2004). RQD of 60%, determined in both cores of boreholes (S40 and S41) and along the eastern slope of the Acquarotta canal, indicates a degree of fracturing which may be responsible, in the gypsum rocky body, for the passage of water and electric current. In this regard, fractures and micro-fractures in crystalline rock constituents are the main transport path for ground water and electric current (Magnusson and Duran, 1984). Furthermore, laboratory tests indicate that the resistivity from dry to moist samples containing gypsum, decreases by orders of magnitude, with values less than 100 Ω·m for saturated and intensely altered gypsum (Finn et al., 2007).

Guinea et al. (2012) found, after laboratory experiments, that the gypsum–lutite rocks approaches the HS lower bound when lutite is at least 60%, while it gets close to HS upper bound for a lesser fraction. In our case, the HS three-phase system modeling includes the water contribution. Within the limitations already discussed, the obtained results near the Acquarotta canal suggest that the HS lower bound is more appropriate than the higher one. This result is quite reasonable since the upper bound better represents cases in which the conductive component resides in unconnected pores, and does not form any continuous conductive paths through the material. This seems physically unrealistic since our investigations involve a subsoil settled below the piezometric surface and because sensible velocity groundwater flow, in a depth fringe several meters thick (up to 9 m) below the sea level (Fidelibus et al., 2011), witness a network of interconnected fractures. It should be stressed that these results are strictly related to water conductivity and its salinity which in turn are influenced by the proximity of the Acquarotta canal. A complete description of chemical analyses of groundwater and surface water samples, in the urbanized area, can be found in Fidelibus et al. (2011). Nevertheless, even assuming a salinity decrease, a further conductive phase (water) must be considered in addition to the lutitic matrix in order to explain the observed resistivities. Therefore, even if a lutite content greater than the observed 20% can't be

Please cite this article as: Festa, V., et al., Geoelectrical resistivity variations and lithological composition in coastal gypsum rocks: A case study from the Lesina Marina..., Eng. Geol. (2016), http://dx.doi.org/10.1016/j.enggeo.2015.12.026

excluded for the whole area, the water content and the mobility of the dissolved ionized solids in the groundwater play a key role in the electrical conductivity enhancement.

Previous studies focused on gypsum rocks have been mainly and successfully carried out in natural dry conditions. The challenging issue of the present work is determined by the unusual geological setting of Lesina Marina, strongly influenced by the presence of water (i.e., lagoon, sea, aquifer and an artificial channel). Henceforth, our findings may be helpful to study the gypsum in similar contexts and to suggest a new framework of susceptibility to the possible occurrence of near-surface collapse phenomena. The cavities, either dissolutional conduits or voids related to gravitational collapse phenomena, i.e., the sinkholes detected in the Lesina Marina area (Melidoro and Panaro, 2000; Fidelibus et al., 2011; Caggiano et al., 2012) seem to characterize mostly the rocky body dominated by massive coarse gypsum (Figs. 2 and 12). Therefore, net of anthropic predisposing and triggering factors (including the gypsum dissolution; e.g. Fidelibus et al., 2011), the development of sinkholes is not restricted to the area of the Lesina Marina village, nor only in the first 30 m in depth. The area with a higher susceptibility to the possible occurrence of sinkholes is much wider, and its width is strongly controlled by the attitude of the massive coarse gypsum rocky body. In the map view (Fig. 12), this area practically corresponds at least to the sector dominated by Quaternary sandy deposits, to the West, and, of course, to the cropping out rocky body dominated by massive coarse grained gypsum, along the Acquarotta canal (Fig. 2). The occurrence of sinkholes cannot be excluded in the areas characterized by the presence of finer grained gypsum rocks (Figs. 2 and 12), which should not be completely free from both paleo-karst and still active dissolution processes.

However, a lower susceptibility to the possible occurrence of near-surface effects due to karst processes can be assigned to these areas (Fig. 12), since the greater resistance shown by the finer grained gypsum rocky body to the development of karst.

6. Concluding remarks

In the Lesina Marina village area, previous studies were mainly concentrated within the urbanized zone and, although well constrained by several drilled logs, limited in depth. In the present paper the first results of an integrated geological mapping, petrographic and geoelectrical investigations, aimed to reconstruct the subsurface geology of the Lesina Marina area, are reported. Sulfate-rich rocks showed to be typified by a wide electrical resistivity range depending on mineral phases of the generic gypsum rocks, hydrogeological and fracturation conditions. The combined effects of all these factors make it impossible to establish a univocal relationship between resistivity and lithology. Nevertheless, the integration of the applied investigation methods allowed us to clearly differentiate the impermeable bedrock from the above rocky body involved by mineral transformations and karstification phenomena. The anhydrite/gypsum transformation and the gypsum dissolution are related to the groundwater circulation starting from the Last Glacial Maximum. These phenomena are spatially localized within the massive coarse grained gypsum rocky body, which dips toward West and Southwest. These findings open new perspectives and suggestion in terms of hazard mitigation. Any program devoted to mitigating the sinkhole risk in Lesina Marina area should, therefore, take into consideration the spatial extent of the damage area together with the factors that might cause it.

Acknowledgments

Four anonymous reviewers are thanked for their useful suggestions, which helped us to improve the manuscript.

We are grateful to the Autorità di Bacino della Puglia for the borehole data, and for the sensitivity shown by this Institution for the geological research in Apulia. This study was financially supported by “Convenzione tra Autorità di Bacino della Puglia e Dipartimento Geomineralogico dell'Università degli Studi di Bari per studi petrografici e mineralogici, oltre che geologico-strutturali, nell'area di Lesina Marina (FG) — 2009” research funds, to V. Festa. The geoelectrical data were partially acquired by Geoprosys s.r.l.

References

Amendolagine, M., Dell'Anna, L., Ventriglia, U., 1964. Le rocce ignee alla Punta delle Pietre Nere presso Lesina (provincia Foggia). Per. Mineral. 33, 337–395.
Antonioli, F., Silenzi, S., 2007. Variazioni relative del livello del mare e vulnerabilità delle pianure costiere italiane. Quad. Soc. Geol. Ital. 2, 1–29.
Bernoulli, D., 2001. Mesozoic–Tertiary Carbonate Platforms, Slopes and Basins of the External Apennines and Sicily. In: Vai, G.B., Martini, I.P. (Eds.), Anatomy of an Orogen: The Apennines and Adjacent Mediterranean Basins. Springer, pp. 307–325.
Berryman, J.G., Hoversten, G.M., 2013. Modelling electrical conductivity for earth media with macroscopic fluid-filled fractures. Geophys. Prospect. 61, 471–493.
Bigalke, J., 2000. A study concerning the conductivity of porous rock. Phys. Chem. Earth Solid Earth Geod. 25 (2), 189–194.
Bigazzi, G., Laurenzi, M.A., Principe, C., Brocchini, D., 1996. New geochronological data on igneous rocks and evaporites of the Pietre Nere Point (Gargano peninsula, southern Italy). Boll. Soc. Geol. Ital. 115, 439–448.
Boni, A., Casnedi, R., Centamore, E., Colantoni, P., Cremonini, G., Elmi, C., Moneto, A., Selli, R., Valletta, M., 1969. Note illustrative alla Carta Geologica d'Italia, F. 155 San Severo. Servizio Geologico d'Italia, Roma, p. 46.
Brady, B.H.G., Brown, E.T., 2006. Rock Mechanics for Underground Mining. Springer, Dordrecht, The Netherlands (628 pp.).
Caggiano, T., Denora, D., Garofalo, G., Versace, P., Di Santo, A., 2012. Zonazione della pericolosità dell'abitato di Lesina Marina - FG. Atti del XXXIII Convegno Nazionale di Idraulica e Costruzioni Idrauliche, Brescia, Italy, p. 10.
Campana, C., Fidelibus, M.D., 2015. Reactive-transport modelling of gypsum dissolution in a coastal karst aquifer in Puglia, southern Italy. Hydrogeol. J. http://dx.doi.org/10.1007/s10040-015-1290-x.
Cardozo, N., Allmendinger, R.W., 2013. Spherical projections with OSXStereonet. Comput. Geosci. 51, 193–205.
Carella, R., 1963. Eruttivi di S. Giovanni in Pane e della Punta delle Pietre Nere (Gargano). Boll. Soc. Geol. Ital. 82, 97–109.
Caterina, D., Beaujean, J., Robert, T., Nguyen, F., 2013. A comparison study of image appraisal tools for electrical resistivity tomography. Near Surf. Geophys. 11, 639–657.
Channell, J.E.T., D'Argenio, B., Horváth, F., 1979. Adria, the African promontory in Mesozoic Mediterranean palaeogeography. Earth-Sci. Rev. 15, 213–292.
Cotecchia, V., Canitano, A., 1954. Sull'affioramento delle Pietre Nere al Lago di Lesina. Boll. Soc. Geol. Ital. 73, 1–16.
Cremonini, G., Elmi, C., Selli, R., 1971. Note illustrative della Carta Geologica d'Italia, scala 1: 100.000, Foglio 156 S. Marco in Lamis. Servizio Geologico d'Italia, Roma, p. 66.
Dahlin, T., Zhou, B., 2004. A numerical comparison of 2D resistivity imaging with 10 electrode arrays. Geophys. Prospect. 52, 379–398.
De Fino, M., La Volpe, L., Piccarreta, G., 1983. Mafic minerals from Punta delle Pietre Nere subvolcanites (Gargano, Southern Italy): their petrological significance. Tschermaks Mineral. Petrogr. Mitt. 32, 69–78.
de Groot-Hedlin, C., Constable, S., 1990. Occam's inversion to generate smooth, two-dimensional models from magnetotelluric data. Geophysics 55, 1613–1624.
Deere, D.U., 1963. Technical Description of Rock Cores for Engineering Purposes. Rock Mechanics and Engineering Geology 1. Springer, p. 18.
Fantoni, R., Franciosi, R., 2010. Tectono-sedimentary setting of Po Plain and Adriatic foreland. Rend. Fis. Acc. Lincei 21 (Suppl. 1), 197–209.
Festa, V., Teofilo, G., Tropeano, M., Spalluto, L., Sabato, L., 2014. New insights on diapirism in the Adriatic Sea: the Tremiti salt structure (Apulia offshore, southeastern Italy). Terra Nova 26, 169–178.
Fidelibus, M.D., Gutiérrez, F., Spilotro, G., 2011. Human-induced hydrogeological changes and sinkholes in the coastal gypsum karst of Lesina Marina area (Foggia Province, Italy). Eng. Geol. 118, 1–19.
Finn, C.A., Deszcz-Pan, M., Anderson, E.D., John, D.A., 2007. Three-dimensional geophysical mapping of rock alteration and water content at Mount Adams, Washington: implications for lahar hazards. J. Geophys. Res. 112, B10204.
Geletti, R., Del Ben, A., Busetti, M., Ramella, R., Volpi, V., 2008. Gas seeps linked to salt structures in the Central Adriatic Sea. Basin Res. 20, 473–487.
Google Earth, 2013, Version 7.1.1, Google Inc., https://www.google.com/earth/.
Griffiths, D.H., Barker, R.D., 1993. Two-dimensional resistivity imaging and modelling in areas of complex geology. J. Appl. Geophys. 29, 211–226.
Guerrero, J., Gutierrez, F., Lucha, P., 2004. Paleosubsidence and active subsidence due to evaporite dissolution in the Zaragoza area (Huerva River valley, NE Spain): processes, spatial distribution and protection measures for transport routes. Eng. Geol. 72, 309–329.
Guinea, A., Playà, E., Rivero, L., Himi, M., Bosch, R., 2010. Geoelectrical classification of gypsum rocks. Surv. Geophys. 31 (6), 557–580.
Guinea, A., Playà, E., Rivero, L., Ledo, J.J., Queralt, P., 2012. The electrical properties of calcium sulfate rocks from decametric to micrometric scale. J. Appl. Geophys. 85, 80–91.
Guinea, A., Playà, E., Rivero, L., Salvany, J.M., 2014. Geoelectrical prospecting of glauberite deposits in the Ebro basin (Spain). Eng. Geol. 174, 73–86.
Gündogan, I., Önal, M., Depçi, T., 2005. Sedimentology, petrography and diagenesis of Eocene–Oligocene evaporites: the Tuzhisar Formation, SW Sivas Basin, Turkey. J. Asian Earth Sci. 25, 791–803.

Please cite this article as: Festa, V., et al., Geoelectrical resistivity variations and lithological composition in coastal gypsum rocks: A case study from the Lesina Marina..., Eng. Geol. (2016), http://dx.doi.org/10.1016/j.enggeo.2015.12.026

Gündogan, I., Helvacı, C., Sözbilir, H., 2008. Gypsiferous carbonates at Honaz Dagi (Denizli): first documentation of Triassic gypsum in western Turkey and its tectonic significance. J. Asian Earth Sci. 32, 49–65.
Hashin, Z., Shtrikman, S., 1963. A variational approach to the theory of the elastic behavior of multiphase materials. J. Mech. Phys. Solids 11, 12–140.
Hermans, T., Vandenbohede, A., Lebbe, L., Martin, R., Kemna, A., Beaujean, J., Nguyen, F., 2012. Imaging artificial salt water infiltration using electrical resistivity tomography constrained by geostatistical data. J. Hydrol. 438-439, 168–180.
Hildyard, R., Prior, D.J., Faulkner, D.R., Mariani, E., 2009. Microstructural analysis of anhydrite rocks from the Triassic evaporites, Umbria-Marche Apennines, Central Italy: an insight into deformation mechanisms and possible slip systems. J. Struct. Geol. 31, 92–103.
Kretz, R., 1983. Symbols for rock-forming minerals. Am. Mineral. 68, 277–279.
Loke, M.H., Barker, R.D., 1996. Rapid least-squares inversion of apparent resistivity pseudosections by a quasi-Newton method. Geophys. Prospect. 44, 131–152.
Loke, M.H., Acworth, I., Dahlin, T., 2003. A comparison of smooth and blocky inversion methods in 2D electrical imaging surveys. Explor. Geophys. 34, 182–187.
Loke, M.H., Chambers, J.E., Rucker, D.F., Kuras, O., Wilkinson, P.B., 2013. Recent developments in the direct-current geoelectrical imaging method. J. Appl. Geophys. 95, 135–156.
Lugo, E., Playà, E., Rivero, L., 2008. Aplicación de la tomografía eléctrica a la prospección de formaciones evaporíticas. Geogaceta 44, 223–226.
Magnusson, K.A., Duran, O., 1984. Comparison between core log and hydraulic and geophysical measurements in boreholes. Geoexploration 22, 169–186.
Manoutsoglou, E., Vachlas, G., Panagopoulos, G., Hamdan, H., 2010. Delineation of gypsum/anhydrite transition zone using electrical tomography. A case study in an active open pit, Altsi, Crete, Greece. J. Balk. Geophys. Soc. 13, 21–28.
Martinis, B., Pieri, M., 1964. Alcune notizie Sulla formazione evaporitica del triassico superiore nell'Italia centrale e meridionale. Mem. Soc. Geol. Ital. 4, 649–678.
Mastronuzzi, G., Sansò, P., 2012. The role of strong earthquakes and tsunami in the Late Holocene evolution of the Fortore River coastal plain (Apulia, Italy): a synthesis. Geomorphology 138, 88–99.
Melidoro, G., Panaro, N., 2000. Sprofondamenti carsici nei gessi costieri di Marina di Lesina (Gargano) e mitigazione del rischio. Geol. Tec. Ambient. 3, 593–606.
Nicolas, R., 2009. JMicroVision: Image Analysis Toolbox for Measuring and Quantifying Components of High-Definition Images, Version 1.2.7. http://www.jmicrovision.com.
Nyquist, J.E., Peake, J.S., Roth, M.J.S., 2007. Comparison of an optimized resistivity array with dipole–dipole soundings in karst terrain. Geophysics 72 (4), F139–F144.
Posenato, E., De Fino, M., La Volpe, L., Piccarreta, G., 1994. L'affioramento del Trias superiore delle Pietre Nere (calcari e gessi) e i prodotti del vulcanesimo basico paleogenico. Guida all'escursione generale precongressuale e alla escursione tematica sul Cretaceo murgiano – 77a Riunione Estiva, Congresso Nazionale della S.G.I., Geologia delle aree di avampaese, pp. 19–23.
Ricchetti, G., Ciaranfi, N., Luperto Sinni, E., Mongelli, F., Pieri, P., 1988. Geodinamica ed evoluzione sedimentaria e tettonica dell'Avampaese Apulo. Mem. Soc. Geol. It. 41, 57–82.
Revil, A., Karaoulis, M., Johnson, T., Kemna, A., 2012. Review: some low-frequency electrical methods for subsurface characterization and monitoring in hydrogeology. Hydrogeol. J. 20, 617–658.
Robert, T., Dassargues, A., Brouyère, S., Kaufmann, O., Hallet, V., Nguyen, F., 2011. Assessing the contribution of electrical resistivity tomography (ERT) and self-potential (SP) methods for a water well drilling program in fractured/karstified limestones. J. Appl. Geophys. 75, 42–53.
Schreiber, B.C., Babel, M., Lugli, S., 2007. Introduction and Overview. In: Schreiber, B.C., Lugli, S., Babel, M. (Eds.), Evaporites Through Space and Time. Geological Society, London, Special Publications 285, pp. 1–13.
Scrocca, D., 2006. Thrust front segmentation induced by differential slab retreat in the Apennines (Italy). Terra Nova 18, 154–161.
Selleri, G., Mastronuzzi, G., 2003. Le aree carsiche gessose d'Italia: Puglia. Ist. Ital. Speleol. Mem. 14 (2), 231–240.
Slater, L., 2007. Near surface electrical characterization of hydraulic conductivity: from petrophysical properties to aquifer geometries—a review. Surv. Geophys. 28, 169–197.
Testa, G., Lugli, S., 2000. Gypsum–anhydrite transformations in Messinian evaporites of central Tuscany (Italy). Sediment. Geol. 130, 249–268.
Zappaterra, E., 1990. Carbonate paleogeographic sequences of the periadriatic region. Boll. Soc. Geol. Ital. 109, 5–20.
Zappaterra, E., 1994. Source-rock distribution model of the periadriatic region. AAPG Bull. 78, 333–354.
Zhou, W., Beck, B.F., Stephenson, J.B., 2000. Reliability of dipole–dipole electrical resistivity tomography for defining depth to bedrock in covered karst terranes. Environ. Geol. 39, 760–766.
Zhou, W., Beck, B.F., Adams, A.L., 2002. Effective electrode array in mapping karst hazards in electrical resistivity tomography. Environ. Geol. 42, 922–928.

Please cite this article as: Festa, V., et al., Geoelectrical resistivity variations and lithological composition in coastal gypsum rocks: A case study from the Lesina Marina..., Eng. Geol. (2016), http://dx.doi.org/10.1016/j.enggeo.2015.12.026